Upper Bound Limit Analysis of Deep Tunnel Face Support Pressure with Nonlinear Failure Criterion under Pore Water Conditions

Zihan Yang * , Yongxin Li , Jingshu Xu

Posted Date: 15 July 2024

doi: 10.20944/preprints202407.1133.v1

Keywords: deep tunnel face; pore water pressure; nonlinear failure criterion; upper bound theorem; failure mechanism; numerical simulation

Article

Upper Bound Limit Analysis of Deep Tunnel Face Support Pressure with Nonlinear Failure Criterion under Pore Water Conditions

Zihan Yang [1,*], Yongxin Li [2] and Jingshu Xu [3]

[1] China Construction Fifth Engineering Division Corp., Ltd., Changsha 410004, China
[2] School of Automotive and Transportation Engineering, Hefei University of Technology, Hefei 230009, China
[3] Key Laboratory of Urban Security and Disaster Engineering, Beijing University of Technology, Beijing 100124, China
* Correspondence: yangkepler@163.com

Abstract: Based on the nonlinear failure criterion and modified tangential technique, the upper bound solutions of supporting pressure on the deep tunnel face were obtained under pore water pressure conditions. The influence of parameters on the supporting pressure and collapse range was investigated according to the unlimited block failure mechanism. It is found that the upper bound solutions of supporting pressure increase with the growth of the nonlinear coefficient and pore water pressure coefficient. The collapse range of the tunnel face scales out with the increase of the nonlinear coefficient and shrinks when increasing the pore water pressure coefficient. Moreover, with the increase of the nonlinear coefficient, the impact strength on supporting pressure and collapse range declines gradually. According to the calculating results, it is manifest that both the pore water pressure and nonlinear criterion factors have negative impacts on the stability of the tunnel face. Thus, more attention should be paid to these parameters to ensure face stability in deep tunnel construction.

Keywords: deep tunnel face; pore water pressure; nonlinear failure criterion; upper bound theorem; failure mechanism; numerical simulation

1. Introduction

The underground environment is complex, indeterminate, and irregular because of the combined effects of many factors, such as complex in situ stress field, composition of rock and soil, underground water, etc. Therefore, it is of great significance for deep tunnel construction to investigate the stability and stress fields under complicated environments. Generally, theoretical analysis, test method, and numerical simulation are three common methods in geotechnical engineering analysis. Classic theoretical analysis approach includes the limit equilibrium method and limit analysis theorem. In the limit analysis approach, it is assumed that rock and soil are ideal elastic-plastic materials and obey the associate flow rule in stability analysis. Researchers from various countries carried out many research works on tunnels using the limit analysis theorem [1-3]. These investigations mainly include two aspects: the vault and side wall stability, and the tunnel face stability. In this paper, the upper bound solutions of tunnel face supporting pressure, which belongs to the latter one, were obtained.

Concerning the study on the tunnel face supporting pressure and failure mechanism, Leca and Dormieux [4] proposed three simple rigid cone failure mechanisms for shallow tunnel faces and calculated the upper bound solution of supporting pressure in clay and friction materials. Soubra [5] improved the failure mechanism by introducing a logarithmic spiral shear block consisting of enormous small cones that were formulated with vertex angles 2φ and a circular bottom surface. Compared with the previous results, this new failure mechanism shows obvious advantages. To consider spatial variability of the soil shear strength parameters for determining the critical collapse pressure

 doi:10.20944/preprints202407.1133.v1

of tunnel faces, Mollon et al. [6] established new 2D and 3D failure mechanisms by means of applying spatial discretization and 'point by point' techniques.

The failure mechanisms of tunnel faces have been gradually improved, and corresponding influencing factors have been introduced into the analysis of these complicated issues. Water, as a predominant element affecting tunnel stability, has received much attention from researchers. Michalowski [7] first considered the pore water pressure as an external force acting on the soil particles and recognized that the work done by the pore water pressure is the sum of the power on the soil deformation and the power on the boundaries. Thus, water factor could be considered in limit analysis theorem. According to Michalowski's research, Huang and Yang [8, 9] derived the collapsing detaching curve functions of tunnel roofs and the corresponding change laws in square and circular tunnels respectively via the upper bound theorem and variation principle under the pore water pressure condition. Zhong et al. [10] and Hou et al. [11] calculated the upper bound solutions of tunnel supporting pressure. The influence of excavation velocity and seepage force on the tunnel face stability was investigated.

In the field of plasticity theory, nonlinear failure criterion is widely adopted. Most of the previous investigations on tunnel stability were based on the Mohr-Coulomb linear failure criterion. However, plenty of tests and theoretical studies have already demonstrated that almost all failure envelopes of geotechnical materials obey nonlinear rule, and that linear condition is merely a special case. In order to introduce nonlinear failure criterion into upper bound theorem, Yang and Yin [12] proposed 'tangent method' to investigate the non-linear characteristics of geo-materials with non-linear SQP algorithm for the optimization of practical projects. For tunnel engineering, Fraldi and Guarracino [13] derived the analytical solution of collapse mechanisms with arbitrary excavation profiles in plastic Hoek-Brown nonlinear rock masses. According to the Power-law nonlinear failure criterion, Yang et al. [14] obtained the upper bound solutions of the supporting pressure in shallow tunnels with optimization theory, and they proposed the modified tangential technique in the meantime.

Excavation of deep tunnel under high pore water pressure condition is still a challenging program for engineers. It is of analytical and practical importance to analyze the stability of deep tunnel with the nonlinear failure criterion. Therefore, under the consideration of pore water pressure and nonlinear failure criterion, the upper bound solutions of deep tunnel face support pressure with a new failure mechanism based on the modified tangential technique were investigated in this paper.

2. Calculation of Supporting Pressure

2.1. Upper Bound Theorem under the Pore Water Pressure Condition

In order to investigate the stability of various geotechnical structures under the pore water pressure condition with limit analysis theory, Viratjandr and Michalowski [15] regarded the power generated by pore water pressure as an external power, so that water factor could be considered in the calculating process of energy dissipation in upper bound theorem. They also held the view that the pore water pressure mainly acts on soil skeletons and the kinematical admissible velocity field boundaries. The specific processes of derivation were shown in Viratjandr's paper, and the final expression for pore water pressure power can be expressed as

$$P_{\mathrm{u}} = -\int_V u\dot{\varepsilon}_{ii}\mathrm{d}V - \int_\Gamma u n_i v_i \mathrm{d}\Gamma \,. \quad (1)$$

where u is the pore water pressure which can be obtained by multiplying pore water pressure coefficient r_{u}, soil weight γ and vertical distance h from a random underground point to the watertable, i.e., $u = r_{\mathrm{u}}\gamma h$. $\dot{\varepsilon}_{ii}$ means the volumetric strain rate and V is the failure mechanism element volume. v_i denotes the velocity vector of kinematical admissible velocity field. n_i represents the outward normal vector on detaching surface and Γ is the failure mechanism boundary.

On the right side of Equation (1), the first part indicates the power generated by pore water pressure acting on soil skeleton and the second part represents the power produced on the boundaries of failure mechanism. Because the failure mechanism adopted in this paper is consisted

 doi:10.20944/preprints202407.1133.v1

of rigid blocks, the geometric deformation is negligible. Therefore, the volumetric strain rate is equal to zero, i.e., $\dot{\varepsilon}_{ii}$=0, which shows that the pore water pressure power is completely composed of the part produced on the failure mechanism boundaries.

According to the upper bound theorem [16], if the hypothetical kinematical admissible velocity field satisfies the displacement boundary conditions, the loads which are obtained by making the external power equal to the energy dissipation rate should be no less than the actual results in limit state. Thus, the formula of the upper bound theorem under the condition of pore water pressure can be acquired.

$$\int_v \sigma_{ij}\dot{\varepsilon}_{ij}\mathrm{d}V \geq \int_\Gamma T_i v_i \mathrm{d}\Gamma + \int_v X_i v_i \mathrm{d}V - \int_\Gamma u n_i v_i \mathrm{d}\Gamma \quad (2)$$

where σ_{ij} and $\dot{\varepsilon}_{ij}$ are the stress tensor and strain rate tensor in a kinematical admissible velocity field, respectively. T_i represents the load acting on the boundary Γ and X_i means the volume force.

2.2. Nonlinear Failure Criterion

2.2.1. Power-Law Nonlinear Failure Criterion

Power-law failure criterion describes the nonlinear relationship between normal stress and shear strength when geotechnical materials reach yield. Because of its simple expression and clear physical meanings, Power-law failure criterion was widely used to solve geotechnical problems [17,18]. The formula can be expressed as follows,

$$\tau = c_0\left(1+\frac{\sigma_\mathrm{n}}{\sigma_\mathrm{t}}\right)^{\frac{1}{m}} \quad (3)$$

where τ and σ_n are the shear strength and normal stress on the detaching surfaces, respectively. Parameter c_0 means the initial cohesion and σ_t represents the tensile strength. Parameter m is the nonlinear coefficient determining the bending degree of the strength envelop. It is obvious that when the nonlinear coefficient m = 1.0, Equation (3) will be degraded into Mohr-Coulomb failure criterion.

2.2.2. Tangent Method in Nonlinear Strength Criterion

Since the strength envelop of nonlinear failure criterion is a curve, it cannot apply the intercept and gradient directly to determine the strength parameters as the linear failure criterion does. In this case, Yang and Yin [9] introduced a tangent on the strength envelop of nonlinear failure criterion and regarded its intercept c_t and gradient φ_t as the equivalent parameters in linear failure criterion conditions. Thus, the nonlinear strength parameters of geotechnical materials were obtained.

As shown in Figure 1, the tangent function is

$$\tau = c_\mathrm{t} + \sigma_\mathrm{n}\tan\varphi_\mathrm{t} \quad (4)$$

where c_t and $\tan\varphi_\mathrm{t}$ represent the intercept and gradient of the tangent respectively, and their formulas can be expressed as follows:

$$c_\mathrm{t} = \frac{m-1}{m}\cdot c_0\left(\frac{m\sigma_\mathrm{t}\tan\varphi_\mathrm{t}}{c_0}\right)^{\frac{1}{1-m}} + \sigma_\mathrm{t}\tan\varphi_\mathrm{t} \quad (5)$$

$$\tan\varphi_\mathrm{t} = \frac{\mathrm{d}\tau}{\mathrm{d}\sigma_\mathrm{n}} = \frac{c_0}{m\sigma_\mathrm{t}}\left(1+\frac{\sigma_\mathrm{n}}{\sigma_\mathrm{t}}\right)^{\frac{1-m}{m}} \quad (6)$$

Preprints.org (www.preprints.org) | NOT PEER-REVIEWED | Posted: 15 July 2024 doi:10.20944/preprints202407.1133.v1

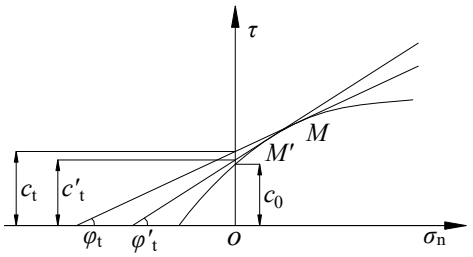

Figure 1. Strength curve based on Power-law nonlinear failure criterion.

2.2.3. Modified Tangential Method

The ordinary approach to obtain the upper bound solutions under the nonlinear conditions is the single tangential method. This method is applied to search for an optimal tangent on the nonlinear strength curve, which can introduce a group of variables (c_t, φ_t) to make the failure mechanism reach the limit state. The single tangential method simplifies the nonlinear failure criterion to a linear one. However, in reality stress field a different normal stress σ_n will lead to various values of variables (c_t, φ_t).

A modified tangential technique [11-14] is proposed based on the single tangential method, with the same formulas of c_t and $\tan\varphi_t$, i.e., Equation (5) and Equation (6). The differences of the variables (c_t, φ_t) subjected to the different stress states are considered in the modified tangential technique which introduces several optimal tangents to make the failure mechanism approach the limit state. In other words, the more optimal tangents with different (c_t, φ_t) are found on the strength envelope, the more accurate the stress field is. In this way, the modified tangential technique is a strict nonlinear analysis method.

2.3. Determination of Failure Mechanism

Referring to the failure mechanism proposed by Lv and Wang [19], the one adopted herein with a number of rigid sliding blocks is shown in Figure 2.

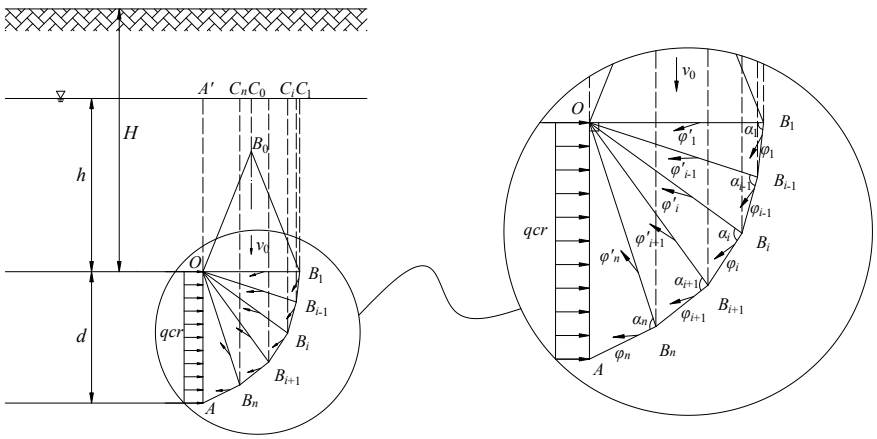

Figure 2. Failure mechanism of deep tunnel face.

The upper part of this mechanism is an isosceles triangle with a $2\varphi_0$ vertex angle, and it has the vertical down direction v_0. Parameter φ_0 is an unknown variable that needs to be optimized and it represents the internal frictional angle under its current stress state conditions. The lower part is consisted of rigid triangle blocks with the vertex angle of same size $\frac{\pi}{2n}$. The parameters φ_i and φ'_i represent internal frictional angles in each rigid triangle block and are determined by its own stress states. They need to be optimized. h represents the vertical distance from the tunnel vault to the water table, and d means the tunnel span.

Preprints.org (www.preprints.org) | NOT PEER-REVIEWED | Posted: 15 July 2024 doi:10.20944/preprints202407.1133.v1

2.4. Process of Calculating Supporting Pressure

The numerical relationships between each velocity vector can be determined by the trigonometric equations expressed in Figure 3. The velocity v_i and $v_{i-1,i}$ represent the absolute and relative velocity of each rigid triangle sliding block respectively.

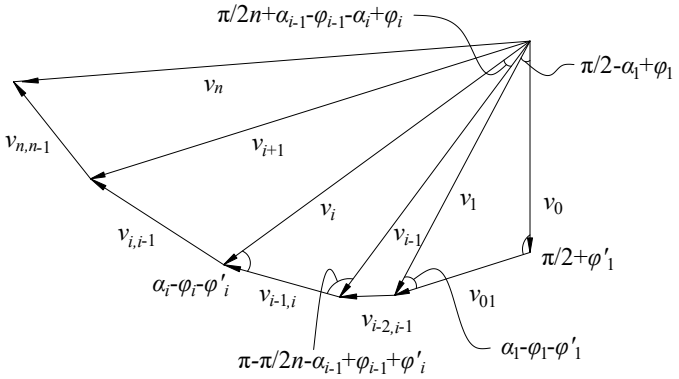

Figure 3. Velocity vectors relationship between triangle blocks.

$$v_1 = \frac{\sin\left(\frac{\pi}{2}+\varphi_1'\right)}{\sin\left(\alpha_1-\varphi_1-\varphi_1'\right)}v_0,$$

$$v_{01} = \frac{\sin\left(\frac{\pi}{2}-\alpha_1+\varphi_1\right)}{\sin\left(\alpha_1-\varphi_1-\varphi_1'\right)}v_0,$$

$$v_i = \frac{\sin\left(\pi-\frac{\pi}{2n}-\alpha_{i-1}+\varphi_{i-1}+\varphi_i'\right)}{\sin\left(\alpha_i-\varphi_i-\varphi_i'\right)}v_{i-1},$$

$$v_{i-1,i} = \frac{\sin\left(\frac{\pi}{2n}+\alpha_{i-1}-\varphi_{i-1}-\alpha_i+\varphi_i\right)}{\sin\left(\alpha_i-\varphi_i-\varphi_i'\right)}v_{i-1}. \quad (7)$$

The geometrical relationships between velocity discontinuous lines are:

$$\overline{OB_n} = \frac{\sin\left(\pi-\alpha_n-\frac{\pi}{2n}\right)}{\sin\alpha_n}\overline{OA},$$

$$\overline{AB_n} = \frac{\sin\frac{\pi}{2n}}{\sin\alpha_n}\overline{OA},$$

$$\overline{OB_i} = \frac{\sin\left(\pi-\alpha_i-\frac{\pi}{2n}\right)}{\sin\alpha_i}\overline{OB_{i+1}},$$

$$\overline{B_iB_{i+1}} = \frac{\sin\frac{\pi}{2n}}{sin\,\alpha_i}\overline{OB_{i+1}},$$

$$\overline{OB_0} = \overline{B_0B_1} = \frac{\sin\left(\frac{\pi}{2}-\varphi_0\right)}{\sin\left(2\varphi_0\right)}\overline{OB_1}. \quad (8)$$

Preprints.org (www.preprints.org) | NOT PEER-REVIEWED | Posted: 15 July 2024 doi:10.20944/preprints202407.1133.v1

When calculating the pore water pressure power, we should set auxiliary lines, as shown in Figure 2 with dotted lines. And their formulas can be expressed by the length of velocity discontinuous lines.

$$\overline{B_0C_0} = h - \overline{OB_0} \cdot \cos\varphi_0 ,$$

$$\overline{B_iC_i} = h + \overline{OB_i} \cdot \sin\left[\frac{\pi}{2n} \cdot (i-1)\right],$$

$$\overline{C_0C_1} = \overline{OB_0} \cdot \sin\varphi_0 ,$$

$$\overline{C_iC_{i+1}} = \overline{B_iB_{i+1}} \cdot \sin\left[\frac{\pi}{2n} \cdot (n+i-1) - \alpha_i\right],$$

$$\overline{A'C_i} = \overline{OB_i} \cdot \cos\left[\frac{\pi}{2n} \cdot (i-1)\right] \quad (9)$$

The areas of the rigid sliding blocks and the polygons composed by auxiliary lines, respectively, are

$$S_{\overline{OB_0B_1}} = \frac{1}{2}\overline{OB_0}^2 \cdot \sin 2\varphi_0 ,$$

$$S_{\overline{OB_iB_{i+1}}} = \frac{1}{2}\overline{OB_i} \cdot \overline{OB_{i+1}} \cdot \sin\frac{\pi}{2n},$$

$$S_{\overline{B_0B_1}} = \frac{1}{2}\left(\overline{B_0C_0} + h\right) \cdot \overline{C_0C_1},$$

$$S_{\overline{OB_i}} = \frac{1}{2}\left(\overline{B_iC_i} + h\right) \cdot \overline{A'C_i},$$

$$S_{\overline{B_iB_{i+1}}} = \frac{1}{2}\left(\overline{B_iC_i} + \overline{B_{i+1}C_{i+1}}\right) \cdot \overline{C_iC_{i+1}} \quad (10)$$

The self-weight power can be expressed as

$$P_\gamma = S_{\overline{OB_0B_1}} \cdot \gamma \cdot v_0 \cdot + \sum_{i=1}^{n} S_{\overline{OB_iB_{i+1}}} \cdot \gamma \cdot v_i \cdot \cos\left[\frac{\pi}{2n}(n+i-1) - \alpha_i + \varphi_i\right] \quad (11)$$

Considering the pore water pressure as an external force, its power acting on the failure mechanism boundaries is

$$P_u = r_u r \cdot \left[2S_{\overline{B_0B_1}} \cdot v_0 \cdot \sin\varphi_0 + \sum_{i=1}^{n} S_{\overline{OB_i}} \cdot v_{i-1,i} \cdot \sin\varphi_i' + \sum_{i=1}^{n} S_{\overline{B_iB_{i+1}}} \cdot v_i \cdot \sin\varphi_i\right] \quad (12)$$

The supporting pressure power results

$$P_{qrc} = \overline{OA} \cdot v_n \cdot \sin\left(\pi - \frac{\pi}{2n} - \alpha_n - \varphi_n\right) \quad (13)$$

The energy dissipation rate on the velocity discontinuous lines can be expressed as

$$P_v = 2\overline{OB_0} \cdot c_0' \cdot v_0 \cdot \cos\varphi_0 + \sum_{i=1}^{n} \overline{OB_i} \cdot c_i' \cdot v_{i-1,i} \cdot \cos\varphi_i' + \sum_{i=1}^{n} \overline{B_iB_{i+1}} \cdot c_i \cdot v_i \cdot \cos\varphi_i \quad (14)$$

where c_0' is the cohesion parameter corresponding to the internal frictional angle φ_0 on the upper part of the failure mechanism, which is different from the initial cohesion c_0.

According to the virtual principle that the power generated by external forces is equal to the internal energy dissipation rate, i.e., $P_\gamma + P_u + P_{qcr} = P_v$. By substituting the above formulas, the upper bound solutions of supporting pressure are obtained.

$$q_{cr} = \frac{P_\gamma + P_u - P_v}{\overline{OA} \cdot v_n \cdot \sin\left(\pi - \frac{\pi}{2n} - \alpha_n + \varphi_n\right)} \quad (15)$$

 doi:10.20944/preprints202407.1133.v1

2.5. Constraint Conditions

The significance of the constraint conditions is to ensure that the failure mechanism satisfies the geometric relationships and boundary conditions; that is, the sliding interfaces must be generated within a proper range and that the twisted distortions cannot occur in the rigid triangle blocks. According to the velocity vector relationships shown in Figure 3, the constraint conditions of the failure mechanism are

$$\begin{cases} 0 < \alpha_i < \pi, \\ 0 < \varphi_i,\ \varphi'_i < \dfrac{\pi}{2}, \\ \alpha_i < \alpha_{i+1}, \\ 0 < \dfrac{\pi}{2n} + \alpha_{i-1} - \varphi_{i-1} - \alpha_i + \varphi_i < \dfrac{\pi}{2}, \\ \pi - \dfrac{\pi}{2n} - \alpha_{i-1} + \varphi_{i-1} + \varphi' > 0, \\ \alpha_i + \left(\pi - \alpha_{i-1} - \dfrac{\pi}{2n} \right) < \pi, \\ \alpha_i - \alpha_{i-1} - \dfrac{\pi}{2n} < 0, \\ \overline{OB_i} < \overline{OB_{i+1}}. \end{cases} \tag{16}$$

Because of the adoption of the modified tangential technique and the multi-block failure mechanism, plenty of parameters remain unknown in the process of calculation. Specifically, φ_i, φ'_i and α_i are unknown in each triangle sliding block. Adding the vertex angle φ_0 in isosceles triangle, the sum of the unknown parameters reaches the number of $3n + 1$. The value of them should be determined by optimization.

Moreover, it is necessary to note that the internal frictional angle φ_0 lacks mutual constraint conditions with other unknown parameters except that it should vary from 0 to $\frac{\pi}{2}$. One may not get the global optimal solutions or results that reach convergence from Matlab optimizing process. Therefore, the varying scope of parameter φ_0 is controlled artificially within a relatively smaller range compared with $(0, \frac{\pi}{2})$. The controlling principle is based on the general corresponding relationships between parameters of geotechnical materials. In this paper the variation range of φ_0 is controlled within 10 degrees, so that it not only could accelerate the speed of computing, but also ensure the correctness of the results.

3. Validation of the Proposed Method

To verify the proposed method, a comparison was made to investigate the difference in the results between the simulation method using the FLAC3D software and the proposed method.

Using the FLAC3D numerical program, the shape of the tunnel face collapse range was obtained with the parameters given as follows: γ = 22 kN/m^3, c_0 = 20 kPa, σ_t =40 kPa, h = 20 m, d = 10 m. The numerical model is shown in Figure 4.

Preprints.org (www.preprints.org) | NOT PEER-REVIEWED | Posted: 15 July 2024 doi:10.20944/preprints202407.1133.v1

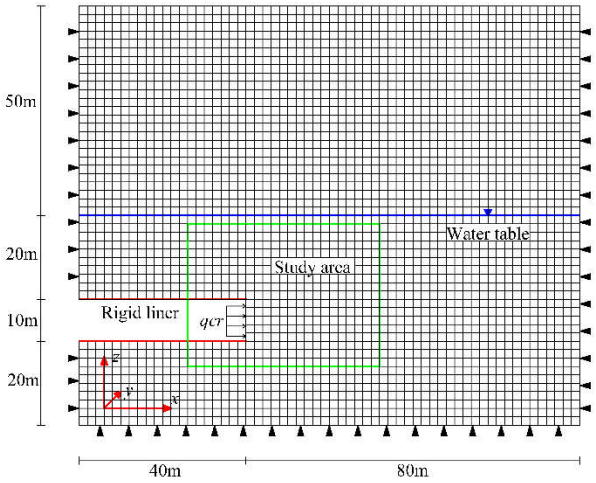

Figure 4. Numerical model of tunnel face in *FLAC*^{3D} software.

To avoid generating disturbed displacement in the computing process, the bottom boundary of the model was fixed in the normal and horizontal directions, and the right and left side boundaries were fixed in the normal direction. Moreover, a horizontal stress of 65kPa was applied in the model to simulate the support pressure on the tunnel face.

Since the Power-low failure criterion was not available in the *FLAC*^{3D} software, the Mohr-Coulomb criterion was adopted in this simulation for simplicity, i.e., m = 1.0. The elastic properties were chosen as the same as the article of Mollon [3], i.e., E = 240 MPa and ν = 0.22, since the collapse shape and range rather than the stress field were more concerned in the plastic collapse state. In addition, a very high value of the elastic modulus E can greatly stimulate the computation speed. The displacement in the vertical direction around the tunnel face is presented in Figure 5.

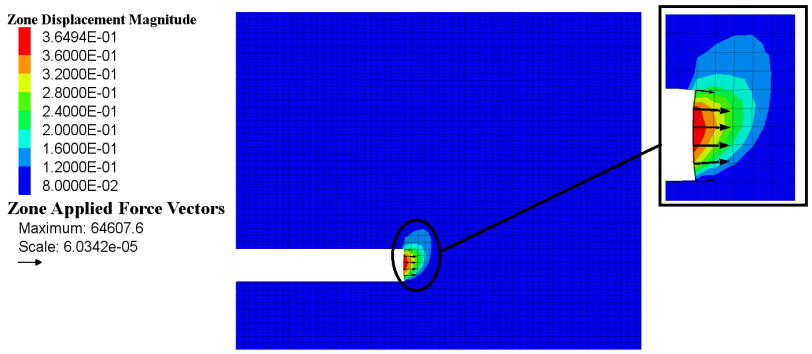

Figure 5. Displacement field in vertical direction around tunnel face.

It was manifest from Figure 5 that the shape of a large deformation area is consistent with the failure mechanism adopted in this paper, which can verify its reasonableness. Moreover, the displacement varies significantly at the top and the bottom of the tunnel face. This is because the boundary conditions change dramatically in these positions; therefore, it is easy to generate the stress concentration phenomenon.

4. Results and Discussion

4.1. Comparison with Theoretical Results

Lv and Wang [19] investigated the stability of the shield tunnel face and calculated the supporting pressure by means of limit analysis and limit equilibrium theory respectively. They found that when the soil internal frictional angle $\varphi > 20^{o}$, the tunnel depth ratio has little effect on the value of supporting pressure, which is consistent with the finite element simulation results by Vermeer et

 doi:10.20944/preprints202407.1133.v1

al. [20]. The reason is that in a deep tunnel the failure surface cannot extend to the ground due to the soil arching effect, and consequently the increase of overlying soil thickness does not continuously increase the magnitude of the supporting pressure.

Identical parameters are used in this paper, γ = 17 kN/m^3, d = 10 m, c_0 = 2 kPa, and the number of rigid sliding blocks refers to n = 9. Furthermore, since Lv and Wang [19] adopted Mohr-Coulomb yield criterion and did not consider the pore water pressure factor, the nonlinear coefficient m and the pore water pressure coefficient r_u here should be equal to 0 and 1.0 respectively. The comparison results are shown in Table 1.

Table 1. Comparison of the calculating solutions with the results by Lv and Wang [19].

Internal frictional angle, φ/º	Supporting pressure by Lv and Wang [19], q/kPa	Supporting pressure in this paper, q/kPa
20	47.59	49.8192
25	35.38	36.6889
30	25.71	26.0332
35	18.69	18.7667
40	14.74	14.7491

It is clear from Table 1 that under the same parameter conditions the two values of supporting pressure are fairly close to each other. Furthermore, with the increase of the internal frictional angle, the differences between these two results tend to diminish. When φ approaches to 40 degrees, the difference is about 9Pa. In general, the similar results demonstrate the feasibility of the new failure mechanism and the correctness of computing process.

4.2. Influence of Triangle Blocks Quantity on Supporting Pressure

In the new failure mechanism, the number of triangle rigid blocks is variable, and their quantity directly impacts on magnitude and accuracy of the supporting pressure. Therefore, to study the influence of the triangle blocks quantity on supporting pressure, the corresponding parameters are: h = 20 m, γ = 22 kN/m^3, d = 10 m, r_u = 0.3, c_0 = 20 kPa, σ_t = 40 kPa. While the values of nonlinear coefficients m are 1.0, 1.4, 1.8, 2.2, 2.6 respectively. The upper bound solutions of supporting pressure with different nonlinear coefficients are calculated and shown in Table 2.

Table 2. Supporting pressure with different triangle block numbers and nonlinear coefficients (Unit: kPa).

Nonlinear coefficient, m	Rigid triangle block numbers, n							
	1	2	3	4	5	6	7	8
1.0	116.4443	113.9599	115.6726	115.4698	114.8485	115.1002	114.4105	114.3245
1.4	134.9470	128.4984	127.2792	128.4241	127.5683	126.9878	126.9342	126.4257
1.8	148.2151	142.8174	138.7556	138.1773	138.4983	137.8676	136.9791	136.5215
2.2	156.3417	151.9835	148.2910	146.0036	145.5345	145.3620	144.6967	143.8646
2.6	161.7502	158.1695	154.7465	152.4798	150.8689	150.4718	149.9788	149.2259

Table 2 shows that when the failure mechanism has a few triangle blocks, ranging from 1 to 4, the values of the supporting pressure fluctuate. With the continuous increase in the number of triangle blocks, the supporting pressure value gradually decreases and stabilizes at the end. When the triangle block number reaches 6 and 7, it is found that under the conditions of distinct nonlinear coefficients, the differences between the values of supporting pressure remain within 1.0kPa. Thus, the calculating results can be considered as converged, and the feasibility of the new failure mechanism is also proved.

 doi:10.20944/preprints202407.1133.v1

4.3. Influence of the Pore Water Pressure Coefficient on Supporting Pressure

To investigate the influence of pore water pressure on supporting pressure, the parameters chosen in calculations are as follows: h = 20 m, d = 10 m, γ = 22 kN/m^3, c_0 = 20 kPa, σ_t = 40 kPa, n = 9, m varies from 1.0 to 2.6, and the pore water pressure coefficient r_u changes from 0.1 to 0.5. The upper bound solutions of supporting pressure are presented in Figure 6.

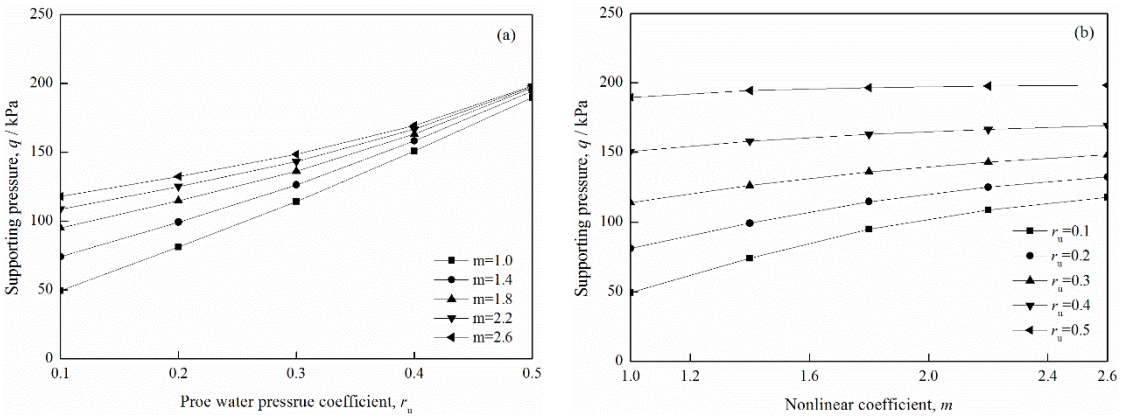

Figure 6. Influence of pore water pressure coefficient and nonlinear coefficient on supporting pressure:(a) Pore water pressure coefficient; (b) Nonlinear coefficient.

From Figure 6 (a), it is found that the value of supporting pressure increases with the increasing number of coefficient r_u, but the increment gradually decreases. When m = 1.0 the value of supporting pressure presents a linear growth. It is consistent with the feature of the Mohr-Coulomb linear failure criterion, which shows the correctness of the calculating results in this paper. Moreover, the influence of nonlinear coefficient m on supporting pressure gradually reduces with the increase of coefficient r_u. For example, in Figure 6 (b) when r_u = 0.5 all the values of supporting pressure with different m remain within the range of 190 to 200 kN.

4.4. Influence of the Underground Water Table Height on Supporting Pressure

In order to study the influence of the underground water table height on supporting pressure, the parameters chosen in calculations are as follows: m = 2.0, d = 10 m, γ = 22 kN/m^3, c_0 = 20 kPa, σ_t = 40 kPa, n = 9, r_u varies from 0.1 to 0.5, and the underground water table height h changes from 20 to 40m. The upper bound solutions of supporting pressure are shown in Figure 5.

It can be found that from Figure 7(a) and Figure 7(b) that with the increase of the water table and the pore water pressure coefficient, the calculating results of supporting pressure show an upward trend. Moreover, when the parameter h is fixed, the value of supporting pressure tends to increase in a form of curve, while the results present the characteristic of linear growth when the parameter r_u is fixed.

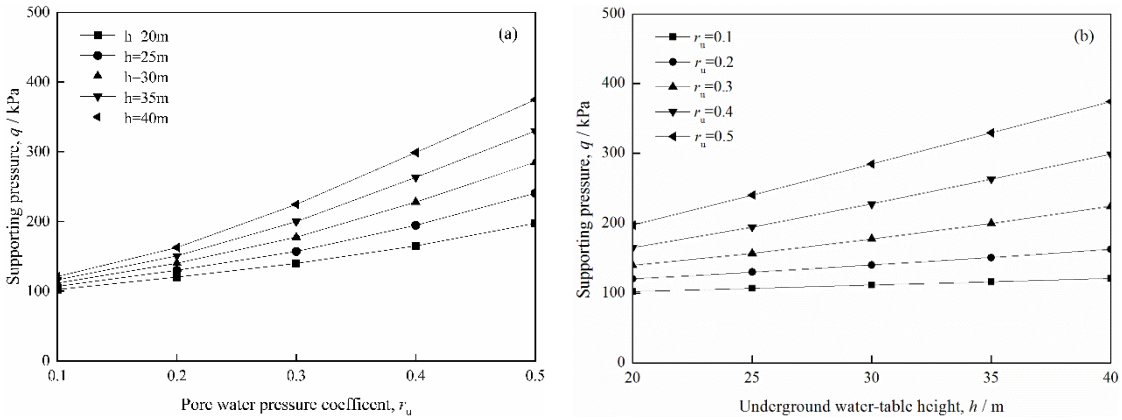

Preprints.org (www.preprints.org) | NOT PEER-REVIEWED | Posted: 15 July 2024 doi:10.20944/preprints202407.1133.v1

Figure 7. Influence of pore water pressure coefficient and water table height on supporting pressure:(a) Pore water pressure coefficient; (b) Underground water height.

4.5. Influence of the Tunnel Span on Supporting Pressure

In order to investigate the influence of the tunnel span on supporting pressure, the parameters in calculations are chosen as follows: γ = 22 kN/m³, c_0 = 20 kPa, σ_t = 40 kPa, r_u = 0.3, h = 20 m, n = 9, m changes from 1.0 to 2.6, and the tunnel span d varies from 6 to 14m. The upper bound solutions of supporting pressure are shown in Figure 6.

It can be seen from Figure 8(a) and Figure 8(b) that the solutions of supporting pressure increase gradually with the growth of tunnel spans and the nonlinear coefficients. Furthermore, one can also see that when the value of tunnel span remains small, such as d = 6 m, the changes of nonlinear coefficient almost have no impact on the supporting pressure. The reason is that tunnels with smaller excavation section height have better stability.

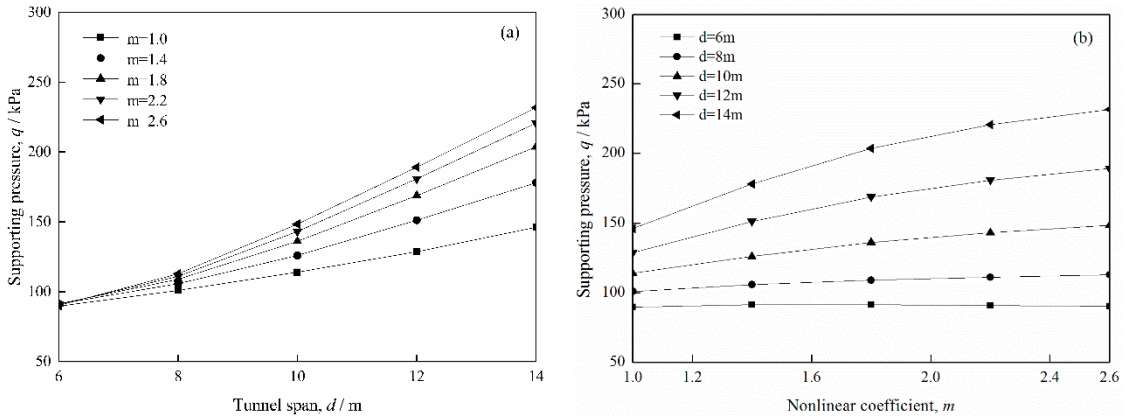

Figure 8. Influence of tunnel span and nonlinear coefficient on supporting pressure:(a) Tunnel span; (b) Nonlinear coefficient.

4.6. Influence of the Nonlinear Coefficient on Collapse Range

In order to estimate the tunnel face collapse range with different nonlinear coefficients, the parameters selected in calculations are: γ = 22 kN/m³, c_0 = 20 kPa, σ_t = 40 kPa, r_u = 0.2, h = 20 m, d = 10 m, n = 9. According to the optimized angles α_i, the collapse ranges are plotted in Figure 7 with nonlinear coefficients m varying from 1.0 to 1.8.

As shown in Figure 9, the collapse range of tunnel face scales out with the increase of nonlinear coefficient, but the expansion decreases gradually. It is consistent with the variations between the nonlinear coefficient and the supporting pressure.

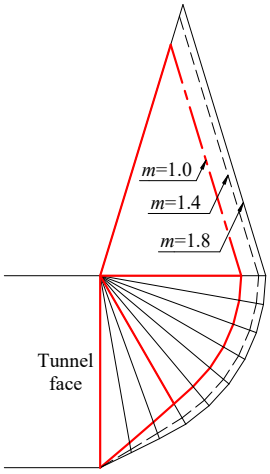

Figure 9. Collapse range with different nonlinear coefficients.

 doi:10.20944/preprints202407.1133.v1

Judging from the overall shape of the collapse range, the failure mode can be divided into three parts-the triangle sections at the bottom, the curved section in the middle and the isosceles triangle section on the top, showing in Figure 9 with bold lines. Furthermore, the shape of the collapse range is similar to the tunnel face failure mechanisms proposed by Mollon [6], which demonstrates that the new failure mechanism adopted in this paper is feasible.

4.7. Influence of the Pore Water Pressure Coefficient on Collapse Range

In order to investigate the collapse range of tunnel face with different pore water pressure coefficients, the parameters in calculations are set as follows: γ = 22 kN/m^3, c_0 = 20 kPa, σ_t = 40 kPa, m = 2.0, h = 20 m, d = 10 m, n = 9. On the basis of optimized angles α_i the collapse ranges are plotted in Figure 10 with r_u varying from 0.1 to 1.5.

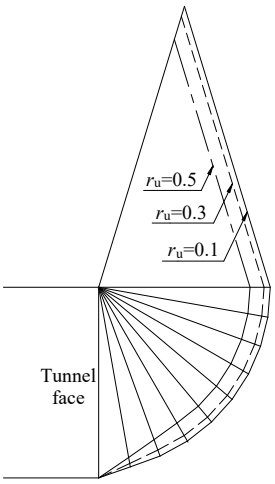

Figure 10. Collapse range with different pore water pressure coefficients.

It shows from Figure 8 that the change law is opposite to that of m, i.e., the tunnel face collapse range shrinks gradually with the increase of pore water pressure coefficient, which is in agreement with the results of Huang [9].

5. Conclusions

A new deep tunnel face failure mechanism with triangle blocks is put forward. According to the nonlinear failure criterion, the upper bound solutions of supporting pressure on a tunnel face are obtained by a modified tangential technique. Compared with previous theoretical results, the correctness of the computing process and the failure mechanism are validated. The formulas of the supporting pressure were deduced.

The influence of different parameters on the supporting pressure is investigated, and the collapse range of the tunnel face is described according to the calculating results. The problem is convergent as the triangle block number in the calculation increases. It is found that the upper bound solutions of supporting pressure increase with the growth of the nonlinear coefficient, pore water pressure coefficient, height of the underground water table, and tunnel span. The collapse range of the tunnel face scales out with the increase of the nonlinear coefficient; however, it shrinks with the increase of the pore water pressure coefficient. Moreover, with the increase of the nonlinear coefficient, the impact strength on supporting pressure and collapse range declines gradually.

In order to avoid the case that the optimizing process cannot converge, the range of parameter φ_0 was restricted on the basis of the general corresponding relationship between parameters. Therefore, the failure mechanism adopted in this paper could be further improved to solve the problem without restricting the parameter φ_0.

Author Contributions: Zihan Yang: Methodology, Validation, Formal analysis, Data curation, Writing, original draft, Visualization. Yongxin Li: Validation, Formal analysis, Data curation, Writing, Original draft. Jingshu Xu: Validation, Formal analysis, Data curation, Writing, Original draft.

 doi:10.20944/preprints202407.1133.v1

Data Availability Statement: The datasets in the current study available from the corresponding author on reasonable request.

Acknowledgements: The preparation of the paper has received financial supports from the National Natural Science Foundation of China (52208409, 52108312, 52208327), Hunan Provincial Natural Science Foundation of China (2022JJ40531) and China State Construction Engineering Corporation Limited Funded Project (CSCEC-2022-Z-16). The financial supports are greatly appreciated.

Conflicts of Interest: The authors declare that they have no known competing financial interests or personal relationships that could have appeared to influence the work reported in this paper.

References

1. Hou, C.T.; Yang, X.L. 3D stability analysis of tunnel face with influence of unsaturated transient flow. *Tunnelling and Underground Space Technology*, **2022**, 123, 104414.
2. Zhong, J.H.; Yang, X.L. Kinematic analysis of the three-dimensional stability for tunnel faces by pseudodynamic approach, *Computers and Geotechnics*, **2021**, 128, 103802.
3. Li, T.Z.; Gong, W.P.; Yang, X.L. Stability analysis of a non-circular tunnel face in soils characterized by modified Mohr-Coulomb yield criterion, **2021**, *Tunnelling and Underground Space Technology*, 109, 103785.
4. Leca, E.; Dormieux, L. Upper and lower bound solutions for the face stability of shallow circular tunnels in frictional material, *Geotechnique*, **1990**, 40(4), 581-606.
5. Soubra, A.H. Three-dimensional face stability analysis of shallow circular tunnels, *International Society for Rock Mechanics, Melbourne: CRC*, **2000**, 19-24.
6. Mollon, G.; Phoon, K.; Dias, D.; Soubra, A. Validation of a new 2D failure mechanism for the stability analysis of a pressurized tunnel face in a spatially varying sand. *Journal of Engineering Mechanics*, **2011**, 137(1), 8-21.
7. Michalowski, R.L. Slope stability analysis: a kinematical approach. *Geotechnique*, **1995**, 45(2), 283-293.
8. Huang, F.; Yang, X.L. Upper bound limit analysis of collapse shape for circular tunnel subjected to pore pressure based on the Hoek-Brown failure criterion. *Tunneling and Underground Space Technology*, **2011**, 26(5), 614-618.
9. Huang, F.; Zhang, D.B.; Sun, Z.B.; Wu, B. Influence of pore water pressure on upper bound analysis of collapse shape for square tunnel in Hoek-Brown media. *Journal of Central South University of Technology*, **2011**, 18(02), 530-535.
10. Zhong, J.H.; Hou, C.T.; Yang, X.L. Three-dimensional face stability analysis of rock tunnels excavated in Hoek-Brown media with a novel multi-cone mechanism. *Computers and Geotechnics*, **2023**, 154, 105158.
11. Hou, C.T.; Zhong, J.H.; Yang, X.L. Three-dimensional stability assessments of a non-circular tunnel face reinforced by bolts under seepage flow conditions. *Tunnelling and Underground Space Technology*, **2023**, 131, 104831.
12. Yang, X.L.; Yin, J.H. Slope stability analysis with nonlinear failure criterion. *Journal of Engineering Mechanics*, **2004**, 130(3), 267-273.
13. Fraldi, M.; Guarracino, F. Analytical solutions for collapse mechanisms in tunnels with arbitrary cross sections. *International Journal of Solids and Structures*, **2010**, 47(2), 216-223.
14. Yang, X.L.; Yang, Z.H.; Li, Y.X.; Li, S.C. Upper bound solution for supporting pressure acting on shallow tunnel based on modified tangential technique. *Journal of Central South University*, **2013**, 20, 3676-3682.
15. Viratjandr, C.; Michalowski, R.L. Limit analysis of submerged slopes subjected to water drawdown. *Canadian Geotechnical Journal*, **2006**, 43(8), 802-814.
16. Chen, W.F. Limit analysis and soil plasticity. *The Netherland: Elsevier*, **1975**, 37-39.
17. Zhang, X.J.; Chen, W.F. Stability analysis of slopes with general nonlinear failure criterion. *International Journal for Numerical and Analytical Methods in Geomechanics*, **1987**, 11(1), 33-50.
18. Li, X. Finite element analysis of slope stability using a nonlinear failure criterion. *Computers and Geotechnics*, **2007**, 34(3): 127-136.
19. Lv, X.L.; Wang, H.R.; Huang, M.S. Limit theoretical study on face stability of shield tunnels. *Chinese Journal of Geotechnical Engineering*. **2011**, 33(1), 57-62. (in Chinese)
20. Vermeer, P.A.; Ruse, N.; Marcher, T. Tunnel heading stability in drained ground. *Felsbau*, **2002**, 20(6): 8-18.